Characteristics of Long Air Gap Discharge Current Subjected to Switching Impulse

Yishi Yue, Hengxin He, Weijiang Chen, *Member, CSEE*, Junjia He, *Member, CSEE*, *Member, IEEE*, Chuanqi Wu, Xiangen Zhao, and Feng Huo

***Abstract*—Measuring the pre-breakdown current of long sparks in air is important for investigating the discharge mechanism. Since the breakdown of long air gaps is conducted by a series of streamer-leader processes, the corresponding current signals cover a bandwidth of 0 to more than 20 MHz. Measurement accuracy of the current from the high voltage side is affected by the displacement current and impulse electromagnetic interference. In this paper, a coaxial current sensor with a DC bandwidth of 74.45 MHz is developed. A displacement current-restrained electrode structure is proposed to reduce the equivalent capacitance between the current sensor and the ground over 30 times. Combined with the digital optical fiber synchronous acquisition unit, a current measurement system for long air gap discharge is established. For the purpose of the UHV system's external insulation optimization design, the discharge current waveform of a 6 m rod-plane air gap under positive switching impulse voltage with 250 μs and 1000 μs time to crest is obtained. Discharge images and stressed voltage are combined to analyze the continuous feature of a current waveform under critical time to crest impulse and discontinuous feature under long front duration impulse. For the purposes of a lightning protection study, the current waveform of a 10 m rod-plane air gap is subjected to negative switching impulse. Finally, the pulse characteristics of the current corresponding to the single channel and branching stepped negative leader are discussed.**

***Index Terms*—Charge density, fluctuation coefficient, leader discharge, long air gap discharge, transient current measurement.**

I. Introduction

MECHANISM research of long air gap discharge is relevant to studies in design optimization of the external insulation of electric power systems [1], [2] and lightning protection [3]–[5]. Conducting long air gap experiments to acquire key physical parameters is the main method for understanding these mechanisms [6]–[8]. Accurate measurements of discharge current under different electrode structures and applied voltages are needed in order to understand the production and migration process of charged particles in long air gap discharges [9]. Many other physical parameters, including the streamer or leader inception voltage, charge density, and space charge volume in long sparks could be derived through an association with other discharge current signals, high-speed discharge images, and applied voltage waveforms.

There are two stages in long air gap discharge: streamer discharge and leader discharge. The streamer discharge produces an impulse current with a short rise-time of 10 to 50 ns, which has a bandwidth of up to tens of MHz. The leader current contains a greater DC component as well as the impulse current that is generated by the streamer in front of the leader. The amplitude of the leader current is related to the polarity of the discharge, ranging from hundreds of mA to hundreds of A. Furthermore, the discharge current can reach several kA during gap breakdowns. Therefore, the long gap discharge current has wide bandwidth characteristics, and a large measurement range. In addition, the current sensor is required to be on the high voltage side and near the discharge electrode in order to exactly measure the current that is produced in the discharge.

The literature in long air gap discharge provides many examples of measurement techniques. The Les Renardières Group employed a resistance sensor and a battery supply oscilloscope operated by technician in a Faraday cage to measure the discharge current in long air gap with bandwidths ranging from 25 Hz to 25 MHz [10]. In [11] and [12], a 17 mΩ shunt was used to measure the leader current of a 16.7 m air rod-plane gap under positive and negative voltage with a bandwidth of 1 MHz and measurements ranging from 3 A to 18 kA to obtain the average discharge current and charge density. In [13] the corona current was measured using a light emitting diode (LED) with a transient response of 10 ns. The Rogowski coil was used to measure positive leader streamer current in [14]. The streamer current of 1 m rod-plane gap was measured using a passive analog signal isolation and transmission system based on the resistance sensor and M-Z electro-optical integrated technology [15]. The discharge current was measured in the high voltage electrode of the sphere-plane gaps [16]. The whole current of conductor and ground wire discharge was measured in a 6 m plane-rod electrode to conductor (ground wire) air gap [17]. In summary, there are three technical problems that need to be investigated to arrive at accurate measurements of the discharge current in long air gap discharge for the whole conductor current:

1) In addition to the current produced by the discharge, current sensor measurements also include displacement

Manuscript received May 15, 2015; revised July 22, 2015; accepted August 22, 2015. Date of publication September 30, 2015; date of current version September 21, 2015. This work was supported by the Fund of the National Basic Research of China (2011CB 209403).

Y. Yue was with State Key Laboratory of Advanced Electromagnetic Engineering and Technology (Huazhong University of Science and Technology), Wuhan 430074, China (e-mail: yueyishi86@sina.com)

H. He, corresponding author, is with State Key Laboratory of Advanced Electromagnetic Engineering and Technology (Huazhong University of Science and Technology), Wuhan 430074, China (e-mail: 76913959@qq.com)

Digital Object Identifier 10.17775/CSEEJPES.2015.00035

current generated by the stray capacitance between the high voltage electrode and the ground. This displacement current should be restrained for accurate measurement of discharge current.

2) A current sensor with wide bandwidth and large measuring range should be fabricated to measure the discharge current.
3) The electrical isolation between high voltage side and ground should be solved. In addition, the influence of the transient electromagnetic interference associated with the applied high voltage on the signal acquisition unit must be determined.

A transient current measurement system with wide bandwidth characteristics and a large measuring range for calculating the discharge current of the whole discharge process is proposed in this paper. The electrode structure is optimized to control the influence of the displacement current; a step response test is performed to evaluate the overall performance of the system. The positive leader discharge current subjected to critical wave front, long wave front, and negative leader discharge current is measured using this system. Combined with the applied voltage and discharge images, the characterstics of measured current are analyzed and the key physical parameters of different experiments are extracted and discussed.

II. Measurement Method

A. Design of Optimized Electrode

The displacement current can be expressed as

$$i_{\mathrm{d}} = C_{\mathrm{str}} \cdot \frac{du}{dt} \tag{1}$$

where C_{str} is the stray capacitance of the gap and du/dt is the rising rate of the applied voltage. The displacement current is reduced by lowering the stray capacitance under a certain voltage waveform. The stray capacitance is related to surface area S of the high-voltage electrode and the gap distance D. Therefore, when the gap distance is chosen, the electrode structure could be optimally designed by decreasing the corresponding superficial area when stray capacitance flows through the current sensor for the purpose of restraining the displacement current. A discharge electrode configuration aimed at decreasing the displacement current is proposed in this paper, as shown in Fig. 1(b). In a typical rod electrode, for example, the current sensor is installed inside the electrode to deflect any serious electromagnetic interference. The main body of the electrode is insulated from the discharge electrode with an insulating plug, preventing the displacement current generated by the main body from flowing through the current sensor. In comparison with an ordinary configuration, the equivalent area related to the displacement current flowing through the current sensor is reduced from S_1 to S_2.

Take the 2 m rod-plane gap for example. The diameter and length of the main body are 36 cm and 6 m, respectively, and the electrode tip is a hemispherical head rod with 7 cm in length and 2 cm in diameter. The stray capacitance is calculated using the COMSOL multi-physics finite element tool to evaluate the effectiveness of the optimal configuration.

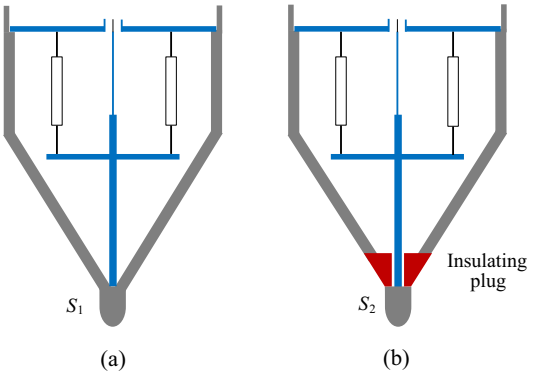

Fig. 1. Schematic diagram of the optimized electrode. (a) Ordinary configuration. (b) Optimal configuration.

The calculated stray capacitance is 74 pF of the ordinary configuration and 1.9 pF of optimal configuration. The results show that the stray capacitance can be reduced by approximately 38 times by using the optimal configuration; the displacement current caused by the stray capacitance thus decreases significantly. Moreover, the optimal method is also suited for any other electrode structures.

The optimal configuration applied in the discharge experiments is shown in the schematic diagram in Fig. 2. Owing to the voltage drop of the current sensor, there is capacitance C_1 between the current sensor and iron shield. When the lead inductance of current sensor L_1 is taken into account, the resistance of current sensor R forms the resonant circuit, and the stray capacitance to the ground forms a resonance loop, which generates an oscillating current signal flowing through the current sensor. In this paper, the damping effect of the current sensor is used to inhibit the high frequency oscillating current.

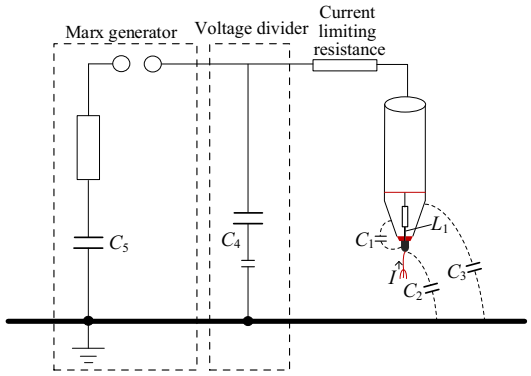

Fig. 2. Schematic diagram of experiment.

The equivalent circuit of the experiment is established to calculate the response of the circuit under different values of current sensor; the range of resistance is obtained by comparing the output signals of the current source and current sensor. The equivalent circuit of the experiment is depicted in Fig. 3, where C_1 is the capacitance between electrode tip and shield, C_2 is the capacitance between electrode tip and ground, C_3 is the capacitance between shield and ground, C_4 is the capacitance of divider, C_5 is the capacitance of Marx

generator, L_1 is the inductance of current sensor, L_2 is the inductance of current sensor lead, L_3 is the inductance of high voltage lead, R_1 is the resistor of current sensor, and R_2 is the resistor of current-limiting resistance.

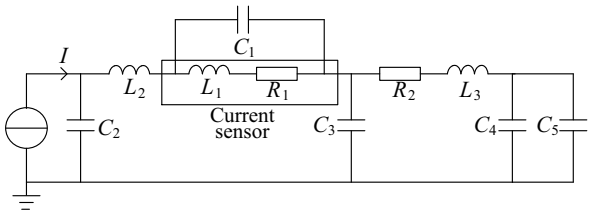

Fig. 3. Equivalent circuit of experiment.

Using the geometric parameters mentioned above, the stray capacitances are calculated as $C_1 = 20$ pF, $C_2 = 1.9$ pF, and $C_3 = 72.1$ pF using COMSOL multi-physics. The capacitances of C_4 and C_5 are 300 pF and 0.3 μF. L_2 is 20 nH calculated using the calculation formula of a straight cylindrical conductor. $L_3 = 10$ μH by using the principle of 1 μH/m, and R_2 is chosen to be 650 Ω. An impulse current with 10 ns wave front and 100 ns wave tail is produced by the current source to simulate the streamer current. The resistances of the current sensor are 5 Ω, 15 Ω, and 35 Ω, and the calculation results are shown in Fig. 4.

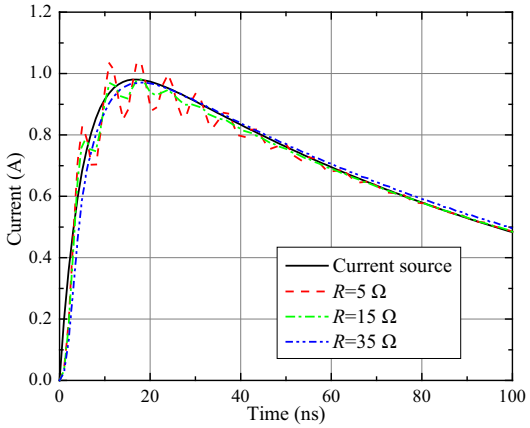

Fig. 4. Calculation results of using different resistances.

The calculation results show that the resistors are effective for diminishing the oscillating current in 2 m gap distance. The relative error between the currents measured in the current source and the current sensor is less than 1%, and the lower limit of the resistor value is 35 Ω. Moreover, the capacitance between electrode tip and ground is reduced to 0.41 pF when the gap distance is 10 m; hence the lower limit could be set to 3 Ω. The resistor value could be chosen using this method in the current measurement under different gap structures.

B. Current Sensor

The current sensor is made up of the inductance-free resistor and the total voltage drop $e(t)$ of the resistor. It contains the resistive and inductive components, which can be given as:

$$e(t) = R \cdot i(t) + L \cdot \frac{di(t)}{dt} \tag{2}$$

where L is the stray inductance of the current sensor. According to the range of the resistor value calculated in Section II. A, a coaxial resistor network consists of several inductance-free resistors in parallel. The magnetic field is zero along the axis because of the vector superposition of the magnetic fields produced by currents flowing through resistors, which can reduce the stray inductances in the resistor network and increase the upper limit of bandwidth.

In the case of a current sensor, which consists of six thick-film-type resistors with resistance of 330 Ω and inductance of less than 60 nH at MHz frequencies, a step response test is used to validate the accuracy and frequency bandwidth of the current sensor. The schematic diagram of the calibration circuit is shown in Fig. 5.

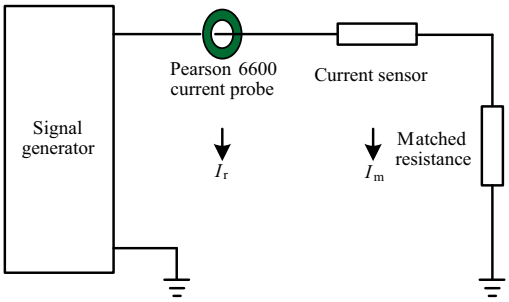

Fig. 5. Schematic diagram of the calibration circuit.

The signal generator used is a high frequency noise generator (SKS-H04GA) with a rise time of less than 5 ns, while the referenced current transducer is a current probe (Pearson current monitor 6600) with a 120 MHz bandwidth. The results of the current probe are recorded using a TDS 3054B oscilloscope (bandwidth of 500 MHz and sampling rate of 5 GS/s).

The step response data are shown in Fig. 6. The error of the current sensor is ± 0.7%. The rise time of the current measured by the current sensor is 4.7 ns, and the bandwidth f_{BW} is given in [18]:

$$f_{\mathrm{BW}} = \frac{0.35}{t_{\mathrm{r}}} \tag{3}$$

where t_{r} is the signal rise time. The bandwidth of the current

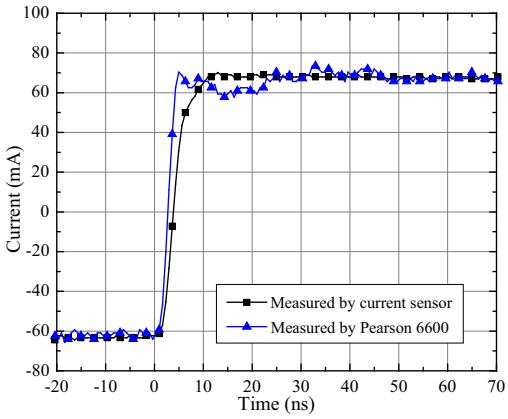

Fig. 6. Step response of the current sensor.

sensor can be calculated as 74.45 MHz, which meets the requirements of current measurement of the long air gap.

C. Synchronous Acquisition Unit

A digital optical fiber synchronous acquisition unit installed in the high voltage side is developed to solve the electrical isolation problem between the high voltage side and ground, and to eliminate the influence of transient electromagnetic interference. The block diagram of the proposed unit is shown in Fig. 7.

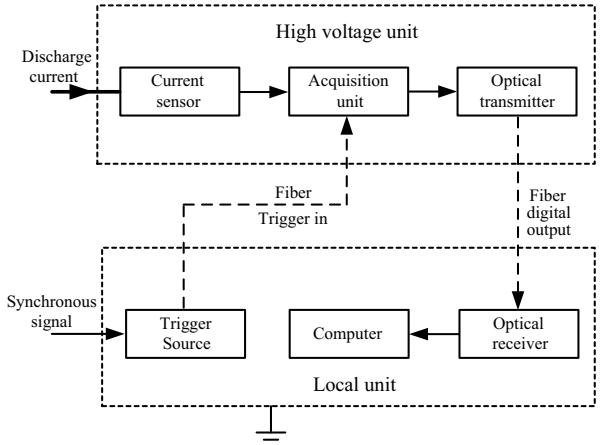

Fig. 7. Block diagram of the digital synchronous acquisition unit.

A high-speed data acquisition card with a 200 MHz bandwidth and 500 MHz sampling rate is chosen. The card acquires the real-time output signal of the current sensor and converts it to a digital signal in the high voltage side. The digital data of the acquisition card are then converted to an optical signal through an optical transmitter and transferred to the local unit in the ground by an optical cable. The high voltage unit is supplied by a storage battery. The optical signal is converted into an electrical signal in the local unit, and the data is then saved in a computer. For simultaneous observation purposes, the external signal is received and converted into an optical signal by the trigger source. The trigger signal is then transmitted to the data acquisition card through an optical fiber to synchronize the current measurement system with other measurement devices. The delay of the trigger signal is 80 ns. The schematic of the current measurement system is shown in Fig. 8.

III. Experimental Setup

A. Experiment Design

Based on the discharge current measurement system mentioned above and combined with the Marx generator and high-speed camera, several discharge experiments under certain conditions were conducted in order to obtain the current waveforms and characteristic parameters of the typical positive and negative discharge. The rod plane air gap was chosen for the experiment as it is the most commonly found geometric structure in power systems. The discharge experiments were as follows:

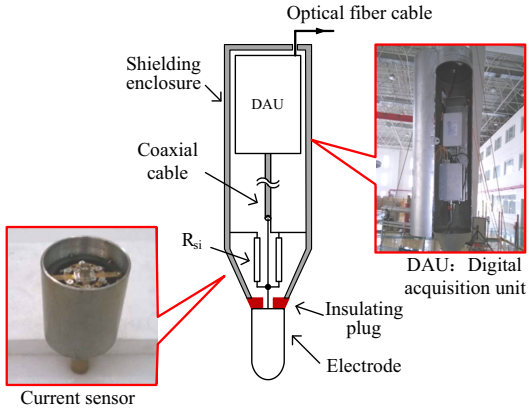

Fig. 8. Schematic of the current measurement system.

1) Positive Leader Discharge Subjected to Critical Wave Front: Many tests have shown that the flashover voltage for various geometrical arrangements under switching voltages decreases by increasing the front time duration of the switching impulse, which can reach the lowest value in the range between 100 and 500 μs [19]. In other words, the critical wave front switching impulse has the minimum breakdown voltage of air gaps. Thus, the critical condition for leader continuous development can be obtained through positive leader discharge research under this condition. According to the critical wave front calculation formula of positive rod-plane gap:

$$T_{\rm cr} = 50(D-1). \tag{4}$$

A 6 m rod-plane gap is adopted and the corresponding critical wave front time is 250 μs using a 250/2500 μs impulse voltage.

2) Positive Leader Discharge Subjected to Long Wave Front: In ultra-high voltage transmission systems, the wave front time reaches up to thousands of μs, which is longer than an extra high voltage system [20]. Research on leader propagation characteristics under long wave front switching impulse makes great sense to the design of external insulation of ultra-high voltage system. The impulse employed in this paper is 1000/2500 μs.

3) Negative Leader Discharge: Negative downward thunderclouds account for 90% of the cloud-to-ground lightning flashes. After the formation of the negative charged thundercloud, the negative stepped leader propagates downwards from the cloud base. Research on the negative leader discharge under critical wave front switching impulse provides a reference for the study of downward leader discharge mechanisms.

$$T_{\rm cr} = 10D. \tag{5}$$

The air gap distance is 10 m, and the 80/2500 μs negative impulse voltage is adopted.

B. Experimental Platform

A schematic diagram of the experimental setup is shown in Fig. 9. The voltage data are measured by the capacitor divider and recorded with a DPO4104B-L oscilloscope. The current is measured using the system proposed in this paper.

A high-speed camera (Photron Fastcam SAX2) with capture maximum parameters of 1000 kilo-frames per second, 1280 × 800 pixel full-resolution is used to observe the optical characteristics of the discharge. The synchronous signal is produced by the oscilloscope.

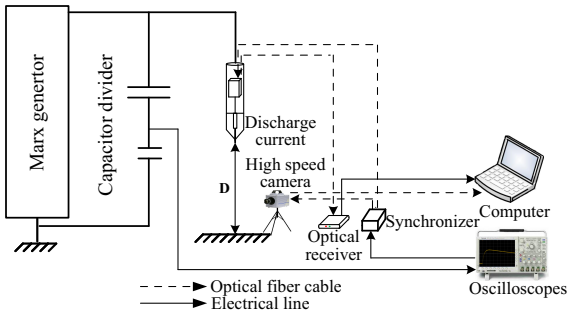

Fig. 9. Schematic diagram of the digital synchronous acquisition device.

IV. Positive Leader Current Subjected to Critical Wave Front

A. Characteristics of Discharge Current Waveform

Typical observation results obtained from 6 m rod-plane gap positive leader discharge experiments are shown in Fig. 10.

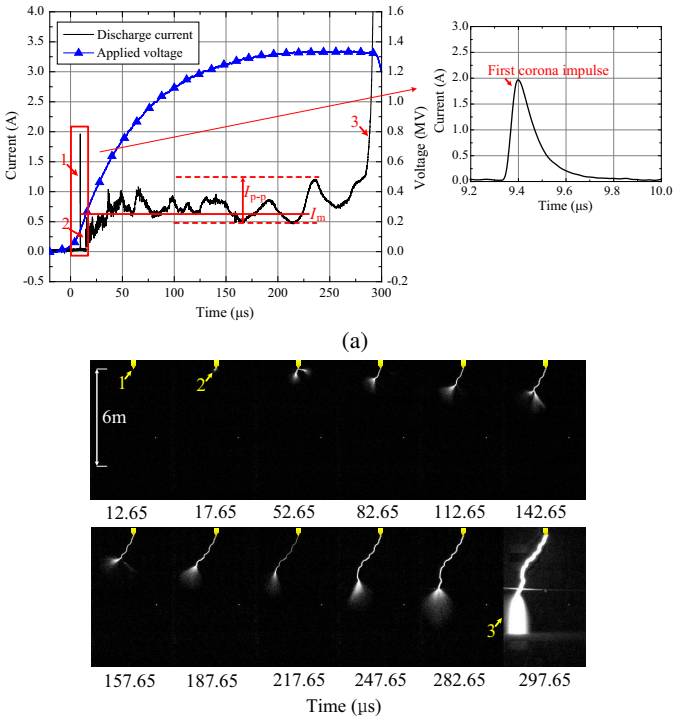

Fig. 10. Observation results of the discharge phenomena in a 6 m rod-plane gap subjected to positive switching impulse under critical wave front. (a) Discharge current and applied voltage. (b) Discharge image.

At $t = 11.75$ μs, the first corona impulse begins. The first corona current impulse is similar to an exponential waveform with 36 ns rise time and 290 ns fall time. Then the current decays to zero without any discharge images because the positive space charge generated by the first corona impulse weakens the electric field of the electrode tip. With an increase in applied voltage, the second corona emerges accompanied by leader discharge at $t = 17.85$ μs. As the electrons generated by the continuous corona discharge of the leader tip flow into the anode through the leader channel, the discharge current is successive in the continuous leader propagation period. The tip of the streamer reaches the plane electrode at $t = 295.62$ μs and the final jump emerges and forms the rod-plane discharge channel resulting in a sudden rise in the current and gap breakdown.

When applying a critical waveform, the leader current is nearly a direct current before the breakdown and the average value I_{m} is 0.69 A. In order to quantify the fluctuation of discharge current waveform, the fluctuation coefficient k is introduced here. It is defined as the ratio between the fluctuation value $I_{\mathrm{p\text{-}p}}$ and average value I_{m} of the leader discharge current shown in Fig. 10 (a). In the example shown in Fig. 10, k is equal to 1.74.

The first corona inception voltage U_{ci}, the leader inception voltage U_{li} and the leader channel charge density q_{L}, all can be acquired through the current waveform. The relationship between q_{L} and the leader propagation velocity v and leader discharge current I can be expressed as follows:

$$q_{\mathrm{L}} = \frac{I}{v}. \tag{6}$$

B. Characteristic Parameters of Discharge Current

The statistical results of the average value of discharge current and fluctuation coefficient among 10 discharge experiments are shown in Table I.

TABLE I
Statistical Results of the Mean Current and Fluctuation Coefficient

Sample Order	Average Current (A)	Fluctuation Coefficient
1	0.77696	1.52444
2	0.75923	1.76220
3	0.62290	2.54524
4	0.67730	1.88325
5	0.71440	1.48818
6	0.69000	1.73913
7	0.74117	1.25255
8	0.79571	1.65780
9	0.86333	1.54212
10	0.70095	2.11829
Standard deviation	0.73	1.75

Statistical results show that the mean value of discharge current and fluctuation coefficient are 0.73 A and 1.75, respectively. The leader inception voltages and correlative first corona inception voltages are listed in Table II.

Measurement results show that the leader inception voltage increases with an increase in the first corona inception voltage. In other words, because of an increase generated in the first corona as inception voltage increases, the leader inception voltage increases in order to gain more energy to offset the shielding effect of the space charge. The relationship between them is approximately linear:

$$U_{\mathrm{li}} = 2.04U_{\mathrm{ci}} - 45.3. \tag{7}$$

TABLE II
FIRST CORONA INCEPTION VOLTAGE AND LEADER INCEPTION VOLTAGE

First Corona Inception Voltage (kV)	Leader Inception Voltage (kV)	First Corona Charge Quantity (μC)
137.94	236.43	0.27
140.59	247.65	0.26
142.69	229.13	0.22
160.08	287.87	0.36
161.94	274.00	0.34
169.16	276.78	0.32
169.29	315.16	0.43
170.94	340.39	0.51
185.01	325.82	0.51
185.02	344.84	0.54

The experimental probability distribution of charge density q_L is reported in Fig. 11. The average charge density is 57.9 μC/m.

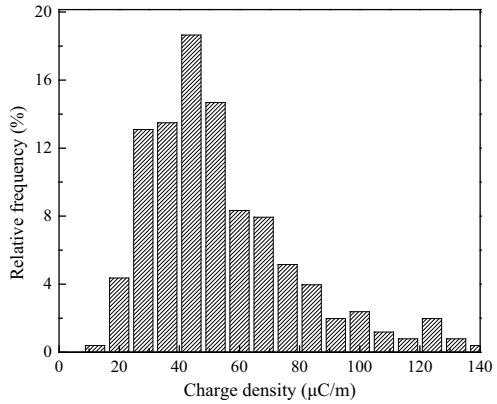

Fig. 11. Probability distribution of charge density.

V. POSITIVE LEADER CURRENT SUBJECTED TO LONG WAVE FRONT

A. Characteristics of Discharge Current Waveform

Typical observation results obtained from a 6 m rod-plane gap subjected to positive switching impulse under 1000 μs wave front are shown in Fig. 12.

Unlike the critical wave front discharge current, the current under a long wave front is in the form of discontinuous impulses. Discharge images indicate that discontinuous impulses are always accompanied by a sudden brightening of the leader channel, which means plenty of electrons are produced by strong ionization activities.

As the increasing rate of applied voltage under long wave front conditions decreases, the increment of the electric field around leader tip is not enough to maintain the continuous development of discharge, so the streamer ionization dies down and the electrons produced by ionization attaches to neutral oxygen molecules when flowing through the branches of streamers.

The leader channel then eventually results in a zero current entering the rod electrode. With an increase in applied voltage, corona incepts again when satisfying the corona inception condition and produces plenty of electrons that is injected into the leader channel that makes the current impulse. Large amounts of photoelectrons are produced during the migration of electrons leading to a sudden brightening of the leader channel. The impulse current before final jump is called "Restrike" [21].

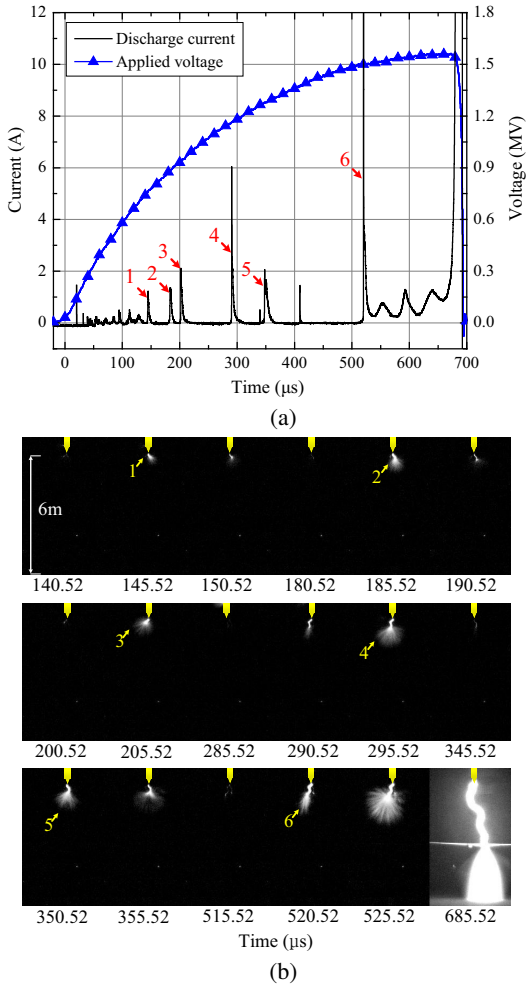

Fig. 12. Observation results of the discharge phenomena in a 6 m rod-plane gap subjected to positive switching impulse under longer wave front. (a) Discharge current and applied voltage. (b) Discharge image.

Two typical impulse current waveforms are found through statistical results of the Restrike current waveform, as shown in Fig. 13.

The wave front time and decline time of the bell-shaped current impulse are almost the same, and the wave front time is 3.8 μs. The wave front time of the double-exponential type is 0.97 μs.

The initial current of the bell-shaped current impulse is not equal to zero because there still exists ionization activities in the streamer zone, and the generated electrons are not completely absorbed by the neutral molecules. The potential of leader tip increases gently because of small increases in the applied voltage, which results in relatively weak ionization activities in the streamer tip. This is similar to the condition of continuous leader propagation. Double-exponential type current has an initial value of zero because there are no ionization activities in the leader tip, which has the same mechanism with streamer discharge. The charge density of

the Restrike current impulse can be acquired indirectly from the measured current waveform.

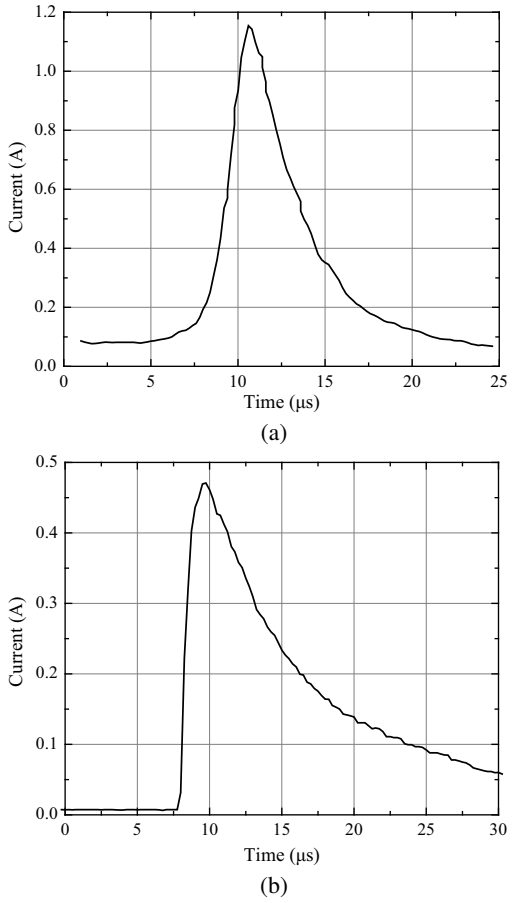

Fig. 13. Typical discharge current of the Restrike. (a) Bell-shaped type. (b) Double-exponential type.

B. Characteristic Parameters of Discharge Current

The charge density probability distribution of 30 Restrikes is reported in Fig. 14. The average charge density of Restrike current impulse is 84.6 μC/m, which is larger than the value under critical wave front circumstances. The reason is that the temperature of leader channel decreases gradually through conduction without the injection of electrons and energy under zero current condition. In addition to heat, the leader tip and the electrons produced by the second corona have to provide the energy needed to improve the temperature of the leader channel so that the average charge density is higher.

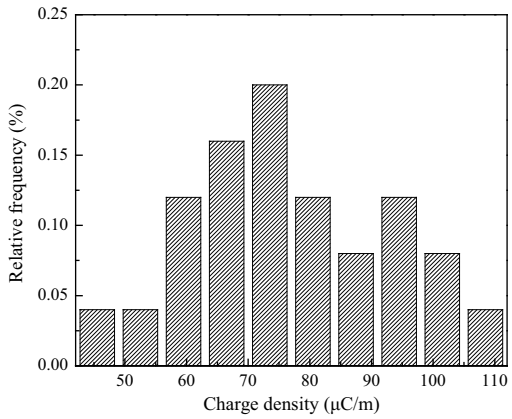

Fig. 14. Probability distribution of Restrike charge density.

VI. Negative Leader Current

A. Characteristics of Discharge Current Waveform

Typical observation results obtained from 10 m rod-plane gap negative leader discharge experiments are shown in Fig. 15.

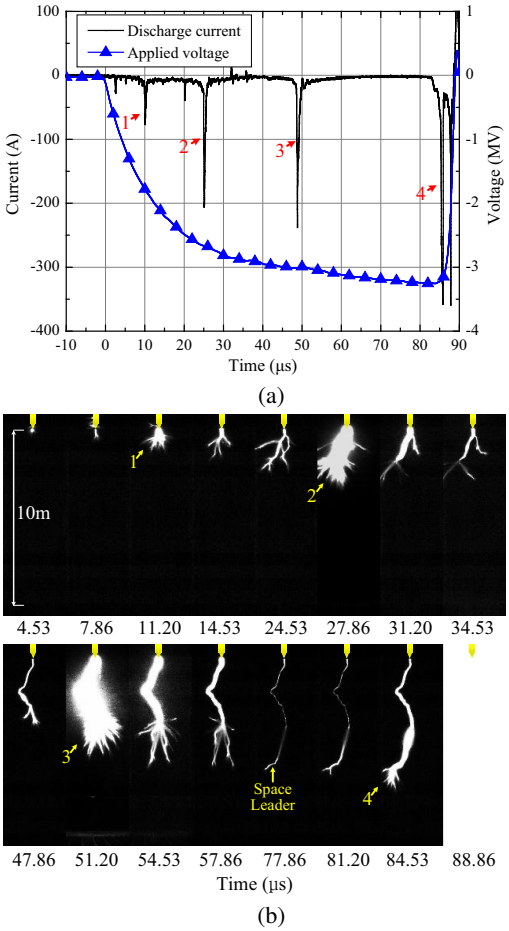

Fig. 15. Observation results of the discharge phenomena in a 10 m rod-plane gap subjected to negative switching impulse. (a) Discharge current and applied voltage. (b) Discharge image.

The negative leader current is in the form of discontinuous impulses, and the peak of the impulse reaches up to several hundred A. Unlike the positive discharge, the electrons produced near the rod electrode move away from the rod under the effect of the background electric field; the positive ions head to the rod electrode, which forms a bi-directional streamer. The electrons generated by the negative streamer move away from the rod so that there is no continuous current. The migrating electrons collide with neutral molecules and transfer part of their kinetic energy resulting in increased temperatures of the neutral molecules and space leader. The positive ions

and electrons gather at both ends of space leader. When the discharge channel from the rod electrode connects with the positive discharge of the space leader, the discharge generates strong luminescence accompanied by a large current impulse and then the main discharge channel elongates until the gap breaks down.

There are two types of negative leader discharge currents, as shown in Fig. 16. The wave front time of single type is 0.28 μs and lasts 0.98 μs while the numbers are 1.18 μs and 2.48 μs, respectively, for the bifurcation type.

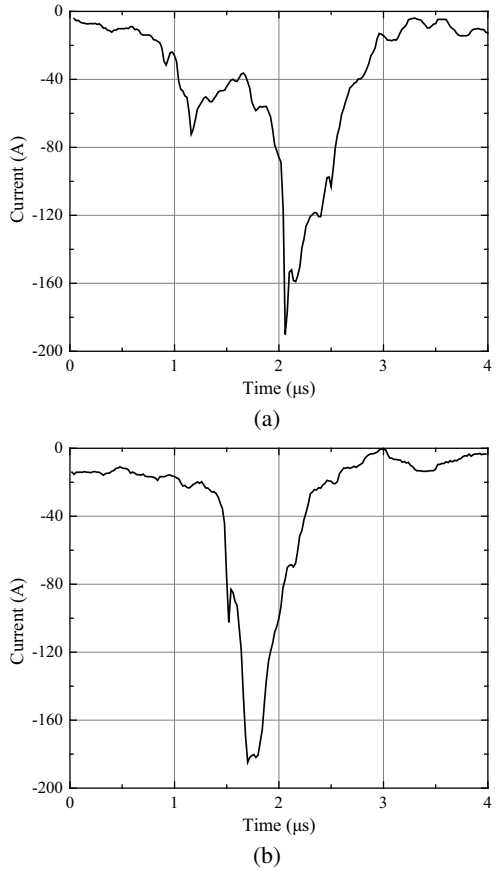

Fig. 16. Discharge current of the typical negative stepped leader. (a) Single type. (b) Bifurcation type.

The bifurcation type leader is formed because the negative leader connects two space leaders simultaneously, as shown in Fig. 17.

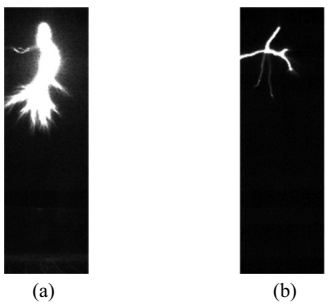

Fig. 17. Type discharge images the typical negative stepped leader. (a) Single type. (b) Bifurcation type.

B. Characteristic Parameters of Discharge Current

The charge density probability distribution of 30 stepped leaders is reported in Fig. 18.

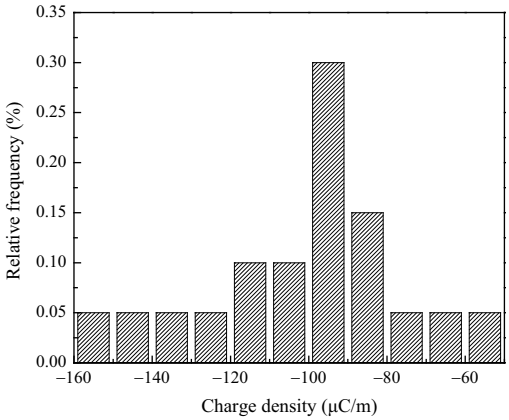

Fig. 18. Probability distribution of stepped leader charge density.

The average charge density of stepped leader is −107.1 μC/m. Its absolute value is larger than the value of positive Restrike, because it is the summation of negative downward streamer charge and the charge of the space leader.

VII. Conclusion

1) An optimized electrode was proposed to reduce the displacement current by 38 times. A coaxial current sensor with 0.7% accuracy and bandwidth from DC to 74.45 MHz was designed. The digital optical fiber synchronous acquisition unit in the high voltage was fabricated. The accurate measurement of discharge current in whole process of long gap discharge can be realized by carrying out these steps.
2) A rod-plane experimental observation system was set up. The statistical average current of 6 m positive discharge subjected to critical wave front time was 0.73 A, the fluctuation coefficient was 1.75. It was found that the leader inception voltage increased with the increase of the first corona inception voltage. The fitting formula between these two parameters were obtained. The extreme probability distribution of charge density was obtained and the average charge density was 57.9 μC/m.
3) Two types of Restrike current impulses with wave front time of 3.8 μs and 0.97 μs, respectively through 6 m rod-plane gap subjected to positive switching impulse under 1000 μs wave front were acquired. The difference in the current type resulted from different degrees of ionization. The charge density probability distribution of Restrike current impulse was obtained, and the average charge density was seen to be 84.6 μC/m, which was larger than the value under the critical wave front circumstance. The reason was that the temperature of leader channel decreases during the Restrike period and needs more energy injected into it to sustain the leader development.
4) Two typical current impulses of negative stepped leader—single type and bifurcation type—were acquired

through 10 m negative discharge experiments. The bifurcation type leader was formed because the negative leader connects two space leaders, simultaneously. The charge density probability distribution of negative stepped leader was obtained and the average charge density was −107.1 μC/m, whose absolute value was larger than the value of positive Restrike because it was the summation of negative downward streamer charge and charge of the space leader.

REFERENCES

[1] Y. Yamagata, A. Oe, K. Miyake, Y. Aihara, T. Shindo, "Phase-to-ground and phase-to-phase sparkover characteristics of external insulation at the entrance of a UHV substation," *IEEE Transactions on Power Delivery*, vol, 17, no. 1, pp. 223–232, 2002.

[2] M. Abdel-Salam and A. Hashem, "Positive corona inception in point-plane gaps as influenced by a surrounding dielectric enclosure," *Journal of Physics D: Applied Physics*, vol. 39, no. 24, pp. 5169–5175, 2006.

[3] U. Kumar, P. K. Bokka, and J. Padhi, "A macroscopic inception criterion for the upward leaders of natural lightning," *IEEE Transactions on Power Delivery*, vol. 20, no. 2, pp. 904–911, 2005.

[4] M. Becerra and V. Cooray, "Time dependent evaluation of the lightning upward connecting leader inception," Journal of Physics D: Applied Physics, vol. 39, no. 21, pp. 4695–4702, 2006.

[5] N. L. Aleksandrov, E. M. Bazelyan E M, Jr R. B. Carpenter, M. M. Drabkin, Y. P. Raizer, , "The effect of coronae on leader initiation and development under thunderstorm conditions and in long air gaps," Journal of Physics D: Applied Physics, vol. 34, no. 22, pp. 3256–3266, 2001.

[6] W. J. Chen, S. Q. Gu, S. J. Xie, S. Bao, H. X. He, J. H. Chen, J. J. He, G. J. Qian, N. W. Xiang, "Experimental observation technology for long air gap discharge," *Proceedings of the CSEE*, vol. 32, no. 10, pp. 13–21, 2012.

[7] W. J. Chen, R. Zeng, H. X. He, "Research progress of long air gap discharge," *High Voltage Engineering*, vol. 39, no. 6, pp. 1281–1295, 2013.

[8] Les Renardières Group, "Positive discharges in long airgaps at Les Renardières 1975 results and conclusions," *Electra*, no. 53, pp. 31–153, 1977.

[9] Les Renardières Group, "Negative discharges in long air gaps at Les Renardières 1978 results," *Electra*, no. 74, pp. 67–216, 1981.

[10] Les Renardières Group, "Research on long air gap discharges at Les Renardières," *Electra*, no. 23, pp. 53–157, 1972.

[11] P. Domens, A. Gibert, J. Dupuy, and B. Hutzler, "Propagation of the positive streamer-leader system in a 16.7 m rod-plane gap," *Journal of Physics D: Applied Physics*, vol. 24, no. 10, pp. 1748–1757, 1991.

[12] P. Ortega, P. Domens, A. Gibert, B. Hutzler, G. Riquel, "Performance of a 16.7 m air rod-plane gap under a negative switching impulse," *Journal of Physics D: Applied Physics*, vol. 27, no. 11, pp. 2379–2387, 1994.

[13] P. Wang and G. Zhang, "The measurement method for corona discharge current under high-voltage environment," *IEEE Transactions on Instrumentation and Measurement*, vol. 57, no. 8, pp. 1786–1790, 2008.

[14] L. Gao, M. Akyuz, A. Larsson, V. Cooray, and V. Scuka, "Measurement of the positive streamer charge," *Journal of Physics D: Applied Physics*, vol. 33, no. 15, pp. 1861–1865, 2000.

[15] Y. N. Geng, R. Zeng, J. L. He, B. Wang, "Pre-breakdown current measurements from high voltage electrode of rod-plane gap under lightning impulse voltage," *High Voltage Engineering*, vol. 37, no. 4, pp. 854–859, 2011.

[16] S. Chen, R, Zeng, C. Zhuang, Z. Q. Yu, J. L. He, "Switching impulse breakdown characteristics of large sphere-plane air gaps compared with rod-plane air gap," *IEEE Transactions on Dielectrics and Electrical Insulation*, vol. 20, no. 3, pp. 839–844, 2013.

[17] Z. Z Li, R. Zeng, Z. Q. Yu, S. Chen, Y. L. Liao, and R. H. Li, , "Research on the upward leader emerging from transmission line by laboratory experiments," *Electric Power Systems Research*, vol. 94, no. SI, pp. 64–70, 2013.

[18] P. R. Gray, P. J. Hurst, S. H. Lewis, and R. G. Meyer, *Analysis and Design of Analog Integrated Circuits*, 5th ed. New York: Wiley, 2009.

[19] A. V. Mytnikov. *High Voltage Engineering*. Tomsk, Russia: Tomsk Polytechnical University, 2012.

[20] Y. Chen, Q. F. Wan, and L. L. Gu, "Research on the long-front switching impulse discharge in UHV tower," *High Voltage Engineering*, vol. 29, no. 11, pp. 21–22, 2003.

[21] I. Gallimberti, G. Bacchiega, A. Bondiou-Clergerie, and L. Philippe, "Fundamental processes in long air gap discharge," *Comptes Rendus Physique*, vol. 3, no. 10, pp. 1335–1359, 2002.

Yishi Yue was born in Shanxi, China, in 1986. He received the B.Sc. degree from Chongqing University, Chongqing, China, in 2008, and the M.Sc. degree from the Huazhong University of Science and Technology, Wuhan, China, in 2010, where he is currently pursuing the Ph.D. degree. His current research interests include long air gap discharge and lightning protection.

Hengxin He was born in Chongqing, China, in 1982. He received the B.Sc., M.Sc., and Ph.D. degrees from the Huazhong University of Science and Technology, Wuhan, China, in 2001, 2005, and 2012, respectively. He is currently a Lecturer with the High Voltage Division, School of Electrical & Electronic Engineering, and the State Key Laboratory of Advanced Electromagnetic Engineering and Technology, Huazhong University of Science and Technology, Wuhan, China. His current research interests include lightning protection, over voltages in power systems, and long air-gap discharge.

Weijiang Chen was born in Shandong Province, China, in 1958. He received the B.Sc. degree from Hefei University of Technology, Hefei, China, and the M.Sc. degree from China Electric Power Research Institute (CEPRI), Beijing, China, in 1982 and 1985, respectively.

From 1985 to 2005, he was with CEPRI, as a Professor. He was the Director of the High Voltage Research Department from 1995 to 2000, and the Vice President of CEPRI from 2000 to 2005. He was appointed the President of Wuhan High Voltage Research Institute from 2005 to 2008. Since 2008, he has been the Vice Director of UHV Department of State Grid Corporation of China (SGCC), taking charge of constructing UHV transmission lines of SGCC. His research interests include overvoltage protection, ultrahigh voltage (UHV) transmission, insulation coordination, surge arrester, and electromagnetic environment in power system. He is the author or coauthor of (TOTAL NUMBER?) books and technical papers.

Professor Chen is the Chairman of HV Professional Committee of Chinese Society for Electrical Engineering (CSEE) and Chairman of China EMC Standardization Technology Committee.

Junjia He was born in Hunan, China, in 1968. He received the B.Sc. and Ph.D. degrees from the Huazhong University of Science and Technology (HUST), Wuhan, China, in 1990 and 1995, respectively. He was a research student with Nagoya University, Nagoya, Japan, from October 1999 to September 2001. Since 2001, he has been a Professor with HUST. His current research interests include high-current high-power pulsed technology and high-voltage engineering. Dr. He is a member of the Institute of Electrical Engineering of Japan and the Society of Chinese Electromechanical Technology.

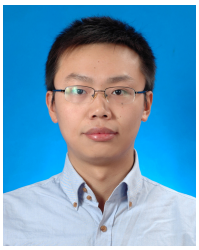

Chuanqi Wu was born in Hubei, China, in 1986. He received the B.Sc. and M.Sc. degrees from the Huazhong University of Science and Technology, Wuhan, China, in 2007 and 2009, respectively. He is currently pursuing the Ph.D. degree. His current research interests include over voltages in power systems, gas discharge, and long air-gap discharge.

Xiangen Zhao was born in Hubei, China in 1989. He received the B.Eng. degree from the Huazhong University of Science and Technology, Wuhan, China in 2011. He is currently a Ph.D. candidate in the School of Electrical and Electronic Engineering, Huazhong University of Science and Technology. His main research interests are the insulation design of power systems and long air gap discharge.

Feng Huo was born in 1979. He received the M.Sc. and Ph.D. degrees from the Wuhan University, Wuhan, China, in 2006 and 2012, respectively.

He is currently a senior engineer with the China Electric Power Research Institute. His main research interests are the external insulation of high voltage, high voltage testing technology, and application of electromagnetic fields.